

Observation of the exceptional point in superconducting qubit with dissipation controlled by parametric modulation

Zhan Wang(王战), Zhongcheng Xiang(相忠诚), Tong Liu(刘桐), Xiaohui Song(宋小会), Pengtao Song(宋鹏涛), Xueyi Guo(郭学仪), Luhong Su(苏鹭红), He Zhang(张贺), Yanjing Du(杜燕京), and Dongning Zheng(郑东宁)

Citation: Chin. Phys. B, 2021, 30 (**10**): 100309. DOI: 10.1088/1674-1056/ac0520
Journal homepage: http://cpb.iphy.ac.cn; http://iopscience.iop.org/cpb

What follows is a list of articles you may be interested in

Quantum speed limit for the maximum coherent state under the squeezed environment

Kang-Ying Du(杜康英), Ya-Jie Ma(马雅洁), Shao-Xiong Wu(武少雄), and Chang-Shui Yu(于长水)
Chin. Phys. B, 2021, 30 (**9**): 090308. DOI: 10.1088/1674-1056/ac0daf

Quantum metrology with coherent superposition of two different coded channels

Dong Xie(谢东), Chunling Xu(徐春玲), and Anmin Wang(王安民)
Chin. Phys. B, 2021, 30 (**9**): 090304. DOI: 10.1088/1674-1056/ac0bae

Quantum multicast schemes of different quantum states via non-maximally entangled channels with multiparty involvement

Yan Yu(于妍), Nan Zhao(赵楠), Chang-Xing Pei(裴昌幸), and Wei Li(李玮)
Chin. Phys. B, 2021, 30 (**9**): 090302. DOI: 10.1088/1674-1056/abeef2

Influences of spin-orbit interaction on quantum speed limit and entanglement of spin qubits in coupled quantum dots

M Bagheri Harouni
Chin. Phys. B, 2021, 30 (**9**): 090301. DOI: 10.1088/1674-1056/abeef4

Optimized pulse for stimulated Raman adiabatic passage on noisy experimental platform

Zhi-Ling Wang(王志凌), Leiyinan Liu(刘雷轶男), and Jian Cui(崔健)
Chin. Phys. B, 2021, 30 (**8**): 080305. DOI: 10.1088/1674-1056/abfccb

---

SPECIAL TOPIC — Non-Hermitian physics

Observation of the exceptional point in superconducting qubit with dissipation controlled by parametric modulation*

Zhan Wang(王战)[1,2], Zhongcheng Xiang(相忠诚)[1], Tong Liu(刘桐)[1,2], Xiaohui Song(宋小会)[1], Pengtao Song(宋鹏涛)[1,2], Xueyi Guo(郭学仪)[1], Luhong Su(苏鹭红)[1,2], He Zhang(张贺)[1,2], Yanjing Du(杜燕京)[1,4], and Dongning Zheng(郑东宁)[1,2,3,†]

[1] *Institute of Physics, Chinese Academy of Sciences, Beijing* 100190, *China*
[2] *University of Chinese Academy of Sciences, Beijing* 100049, *China*
[3] *Songshan Lake Materials Laboratory, Dongguan* 523808, *China*
[4] *China University of Geosciences, Beijing* 100083, *China*

(Received 7 May 2021; revised manuscript received 22 May 2021; accepted manuscript online 26 May 2021)

Open physical systems described by the non-Hermitian Hamiltonian with parity-time-reversal (PT) symmetry show peculiar phenomena, such as the presence of an exceptional point (EP) at which the PT symmetry is broken and two resonant modes of the Hamiltonian become degenerate. Near the EP, the system could be more sensitive to external perturbations and this may lead to enhanced sensing. In this paper, we present experimental results on the observation of PT symmetry broken transition and the EP using a tunable superconducting qubit. The quantum system of investigation is formed by the two levels of the qubit and the energy loss of the system to the environment is controlled by a method of parametric modulation of the qubit frequency. This method is simple with no requirements for additional elements or qubit device modifications. We believe it can be easily implemented on multi-qubit devices that would be suitable for further exploration of non-Hermitian physics in more complex and diverse systems.

Keywords: exceptional point, parity-time-reversal (PT) symmetry, longitudinal field modulation

PACS: 03.67.–a, 03.65.Aa, 03.67.Lx, 03.65.Ta **DOI:** 10.1088/1674-1056/ac0520

1. Introduction

In recent years, non-Hermitian systems with PT symmetry have attracted widespread attention because of their intriguing properties and potential applications in sensitive detection.[1] The PT symmetry can be realized by considering a coupled bipartite system with balanced gain and loss of energy or particles from the environment.[2] By varying the relative magnitude of the gain, loss and coupling strength, the system can show an unconventional transition between a PT symmetric phase and a PT broken phase at a so-called exceptional point (EP). At the EP, the eigenvalues of the non-Hermitian Hamiltonian, which describes the system, coalesce together and the corresponding eigenvectors also coincide at this point. Also, the breaking of the PT symmetry causes the eigenvalues of the non-Hermitian Hamiltonian to change from real to complex. The presence of the EP can lead to many peculiar physical phenomena, such as unidirectional invisibility,[3] nonreciprocal light propagation,[4–7] loss-induced suppression and revival of lasing.[8–10] More importantly, it is suggested that near the EP the system is more sensitive to external perturbations and this could give rise to enhanced sensing.[11,12]

EPs have been experimentally observed in different kinds of systems. Initially, it was mostly reported in semiclassical systems with balanced gain and loss, such as optical cavities,[11–14] microwave resonators[6,15–17] and mechanical oscillators.[18–20] More recently, work performed on quantum systems, such as cold atoms,[21–23] nitrogen-vacancy centers,[24,25] superconducting circuits[26,27] and trapped ions[28,29] were reported. For the pure lossy quantum system, it has been shown that the lossy Hamiltonian could be mapped to a PT symmetric Hamiltonian and display passive PT symmetry breaking.[21,32]

In superconducting circuits, a single transmon qubit embedded in a 3D waveguide cavity is used to demonstrate the PT symmetry broken transition and the presence of EP.[26] The lowest three energy levels $|g\rangle$, $|e\rangle$, and $|f\rangle$ of the qubit are involved. The first excited state $|e\rangle$ and the second excited state $|f\rangle$ are used to form the bipartite quantum system of investigation while the ground state $|g\rangle$ is regarded as the environment. The key to the demonstration of the PT symmetry broken transition is a large and adjustable dissipation channel for a large decay rate of $|e\rangle$ to $|g\rangle$. It is realized by inserting an impedance matching element (IME) between the cavity and

*Project supported by the State Key Development Program for Basic Research of China (Grant Nos. 2017YFA0304300 and 2016YFA0300600), the Key-Area Research and Development Program of Guangdong Province, China (Grant No. 2020B0303030001), and the Strategic Priority Research Program of Chinese Academy of Sciences (Grant No. XDB28000000).

†Corresponding author. E-mail: dzheng@iphy.ac.cn

© 2021 Chinese Physical Society and IOP Publishing Ltd

the outside readout circuit. However, this method requires an additional element that may affect the performance of the entire qubit device. In this work, we demonstrate the observation of the PT symmetric broken phase transition and the EP on a frequency tunable superconducting Xmon qubit by parametric modulation of the qubit frequency that results in a controllable interaction between the qubit and a lossy readout resonator. This interaction transfers the qubit excitation to the resonator and, thus, creates a lossy channel controlling the decay rate of $|e\rangle$ to $|g\rangle$. This approach of decay rate controlling with parametric modulation has been proposed in Ref. [30] and has been used for fast reset of superconducting qubits. It is simple and requires no additional hardware or modifications to the device components. It can be implemented easily on multi-qubit devices for the exploration of rich physics in non-Hermitian systems with PT symmetry.

2. Principle of the experiment

2.1. PT symmetry broken transition in a single dissipative qubit

As shown in Ref. [26], a two-level non-Hermitian system with applied resonance driving and a loss term to the environment may be described by an effective Hamiltonian ($\hbar = 1$)

$$H_{\rm eff} = J(|f\rangle\langle e| + |e\rangle\langle f|) - {\rm i}\frac{\gamma_e}{2}|e\rangle\langle e|, \tag{1}$$

where $|e\rangle$ and $|g\rangle$ denote the first and second excited states of the quantum system, respectively, and γ_e is the occupation-number loss rate. This Hamiltonian may be rewritten as $H_{\rm eff} = H_{\rm PT} - {\rm i}\gamma_e I/4$, where $H_{\rm PT} = J\sigma_x - {\rm i}\gamma_e\sigma_z/4$ is a PT-symmetric Hamiltonian, and I is the identity matrix, $\sigma_{x(z)}$ is the Pauli matrix, $J\sigma_x = J(|f\rangle\langle e| + |e\rangle\langle f|)$ when we just consider the $|e\rangle$ state and the $|f\rangle$ state. The complex eigenvalues of $H_{\rm eff}$ have different imaginary components at $J < \gamma_e/4$, and the system is in the PT broken phase. At a stronger coupling, past the EP at $J_0 = \gamma_e/4$, the imaginary components for the two dissipative eigenmodes coincide, and the system is in the PT symmetric (unbroken) phase. To implement $H_{\rm eff}$, we require the respective energy decay rates $\gamma_e \gg \gamma_f$.

2.2. Qubit decay rate control

We consider a generic system with a two-level atom (with transition frequency $\omega_{\rm q}$) coupled to a resonator (with frequency $\omega_{\rm r}$). If the effective coupling is $g_{\rm eff}$, the Hamiltonian ($\hbar = 1$) of this coupled system in the Jaynes–Cummings model is

$$H_{\rm s} = \frac{\omega_{\rm q}}{2}\sigma_z + \omega_{\rm r}a^+a + g_{\rm eff}(a^+\sigma^- + a\sigma^+), \tag{2}$$

where a, a^+, σ^-, σ^+ are lowering and raising operators of the resonator and the qubit, respectively, and σ_z is the Pauli matrix. Considering the dissipation, the dynamics can be described by the following Lindblad master equation:

$$\dot{\rho} = -{\rm i}[H_{\rm s},\rho] + \frac{\kappa_{\rm r}}{2}D[a]\rho + \frac{\gamma_e^{\rm idle}}{2}D[\sigma^-]\rho, \tag{3}$$

where ρ is the density matrix of the system, $D[x]\rho = 2x\rho x^+ - [x^+x,\rho]$, $\kappa_{\rm r}$ is the photon loss rate of the resonator and $\gamma_e^{\rm idle}$ the decay rate of the state $|e\rangle$ when the qubit is on the idle frequency, which will be discussed in Section 3. Under the condition $\kappa_{\rm r} \gg \gamma_e^{\rm idle}$, the cavity mode can be adiabatically eliminated. Then we obtain

$$\begin{aligned}\dot{\rho} \;=\; & -{\rm i}\frac{\omega_{\rm q}^*}{2}[\sigma_z,\rho] + \frac{\gamma_e^{\rm idle}}{2} \\ & \times\left(1 + \frac{g_{\rm eff}^2\kappa_{\rm r}}{\gamma_e^{\rm idle}(\kappa_{\rm r}^2/4 + \Delta\omega^2)}\right)D[\sigma_z]\rho,\end{aligned} \tag{4}$$

where $\omega_{\rm q}^* = \omega_{\rm q} + g_{\rm eff}^2\Delta\omega/(\kappa_{\rm r}^2/4 + \Delta\omega^2)$. Therefore, the effective decay rate of the qubit is

$$\gamma_e = \gamma_e^{\rm idle} + \frac{g_{\rm eff}^2\kappa_{\rm r}}{\kappa_{\rm r}^2/4 + \Delta\omega^2}. \tag{5}$$

The above formula shows that γ_e can be tuned by varying g_e and the frequency detuning $\Delta\omega$. Obviously, the $\gamma_{\rm e}$ shows maximum when $\Delta\omega = 0$.

2.3. Longitudinal field modulation

For a single Xmon, we realize qubit frequency parametric modulation by applying a longitudinal field modulation (LFM) with frequency ω_z and amplitude h_z. In the laboratory coordinate system, the Hamiltonian ($\hbar = 1$) of the qubit system with LFM and transverse resonance driving is

$$H = \omega_{\rm q}\sigma^+\sigma^- + h_z\cos(\omega_z t)\sigma^+\sigma^- + \Omega_x\sigma_x. \tag{6}$$

Under the rotating wave approximation and note

$${\rm e}^{{\rm i}\alpha\sin(\omega t)} = \sum_{n=-\infty}^{n=\infty} J_n(\alpha)\,{\rm e}^{{\rm i}n\omega t}. \tag{7}$$

The Hamiltonian may be expressed as

$$H_1 = (\omega_{\rm q} - n\omega_z)\sigma^+\sigma^- + \Omega_x J_n\left(\frac{h_z}{\omega_z}\right)\sigma_x, \tag{8}$$

where J_n is the nth-Bessel functions of the first kind. It shows, with the LFM applied on the qubit, sidebands appear at $\omega_{\rm q} - n\omega_z$ ($n = 0, \pm1, \pm2, \ldots$). Another feature of the Hamiltonian is that the Rabi oscillation term may disappear when $J_n(\alpha) = 0$. In Fig. 1, we show the measured qubit energy spectrum with and without LFM. The measurements are taken at $\omega_{\rm q}/2\pi \sim 4.92$ GHz and $\omega_z/2\pi = 0$, 20 MHz.

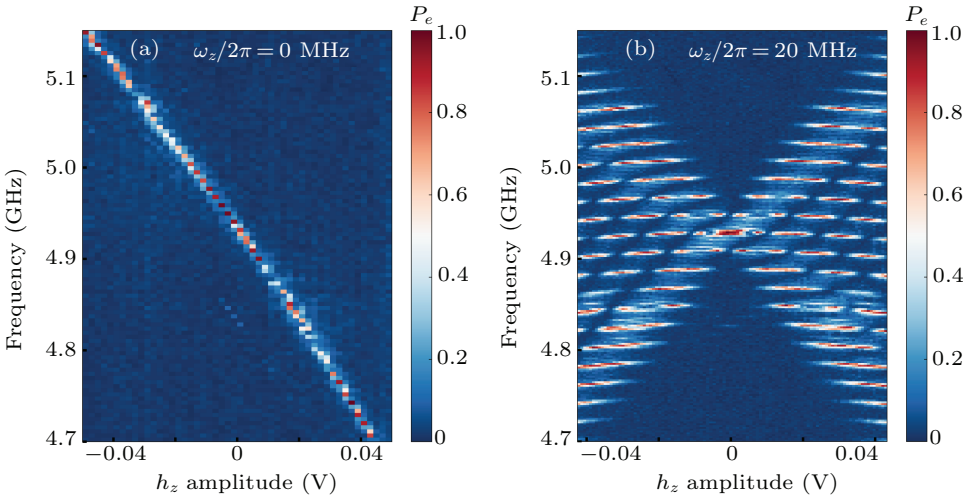


Fig. 1. Measured qubit energy spectrum (a) without and (b) with LFM. The qubit is biased at 4.92 GHz. The modulation frequency is $\omega_z/2\pi = 20$ MHz.

3. Experimental setup

In the experiment, we realize a non-Hermitian system with PT symmetry on a frequency tunable superconducting Xmon qubit. Figure 1(a) shows an optical photograph of the device. The qubit is formed by a DC-SQUID (the enlarged region in the graph) shunted by a cross-shaped capacitor. The Xmon qubit can be regarded as an anharmonic oscillator exhibiting a series of unequally spaced energy levels that can be individually addressed with microwave pulses via the XY control line. A magnetic flux applied to the SQUID loop through the Z control line can tune the energy level spacing. The qubit is capacitively coupled to a readout $\lambda/4$ resonator that is also coupled to a microwave transmission line. When the fundamental mode frequency of the resonator is substantially larger than the qubit transition frequency between the lowest two levels, the dispersive interaction between the qubit and the resonator results in a state-dependent shift in the resonator frequency. Thus, in this dispersive readout scheme, the qubit state information can be obtained by measuring the transmission or reflection coefficients of the transmission line.

Following the scheme of Ref. [26], we use the first two excited states of $|e\rangle$ and $|f\rangle$ to form a two-level system and regard the ground state $|g\rangle$ as the environment. By applying a coherent resonate drive (Rabi drive) of variable amplitude, the coupling between $|e\rangle$ and $|f\rangle$ can be realized. To observe the PT symmetry broken transition and the EP, we need to introduce controllable losses of the system energy to the environment in such a way that the decay rate of the state $|e\rangle$ (γ_e) is much larger than that of the state $|f\rangle$ (γ_f). This can be realized by parametric modulation of qubit frequency using LFM as discussed in Subsection 2.3. In other words, when the frequency of one sideband is in resonance with the readout resonator, the decay through the lossy readout resonator is maximized. By varying the LFM frequency and amplitude, the decay can be adjusted. Meanwhile, we vary the driving amplitude Ω_x, which means changing the coupling strength J, so that the PT symmetry broken transition can be observed. The schematic of this process and the corresponding pulse and waveform sequence are shown in Figs. 2(b) and 2(c).

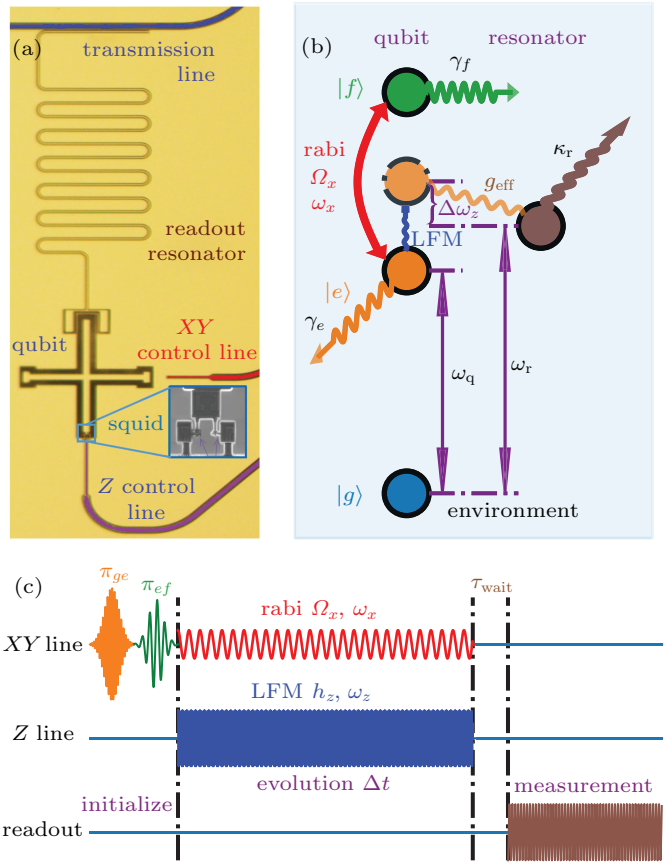


Fig. 2. (a) Optical graph of a frequency tunable superconducting Xmon qubit. (b) Experiment schematic diagram for the observation of the PT symmetry broken transition and the EP. In the diagram, γ_e, γ_f, κ_r represents the decay rate of the states $|e\rangle$, $|f\rangle$ and the resonator, respectively. The g_{eff} and $\Delta\omega$ are the effective coupling strength and detuning between the resonator and the qubit after applying longitudinal field modulation (LFM). Ω_x is the amplitude of Rabi driving while ω_x is the frequency. ω_r and ω_q are the frequencies of the resonator and the qubit (energy level between the state $|g\rangle$ and $|e\rangle$), respectively. (c) Pulse and waveform sequence of the experiments.

To ensure that the experimental conditions meet the theoretical requirements, characterization work needs to be carried out at first. Initial state preparation and readout are carried out at an idle frequency point, corresponding to $\omega_{ge}/2\pi = 5.69378$ GHz and $\omega_{fe}/2\pi = 5.4411$ GHz. The anharmonicity is about 252.67 MHz. The readout resonator frequency is about 6.6178 GHz and it differs from the $\omega_{ge}/2\pi$ by 924 MHz. The readout resonator frequency shift $2\chi_{ge}$ is about 0.55 MHz when the qubit is excited from $|g\rangle$ to $|e\rangle$ while the shift $2\chi_{ef}$ is about 0.4 MHz for $|e\rangle$ to $|f\rangle$ excitation. The coupling strength between the qubit and the readout resonator may be calculated from the shift value and is found to be ~ 48.7 MHz. With the AC stark effect measurements, the decay rate of photons in the readout resonator κ_r is ~ 6 MHz.

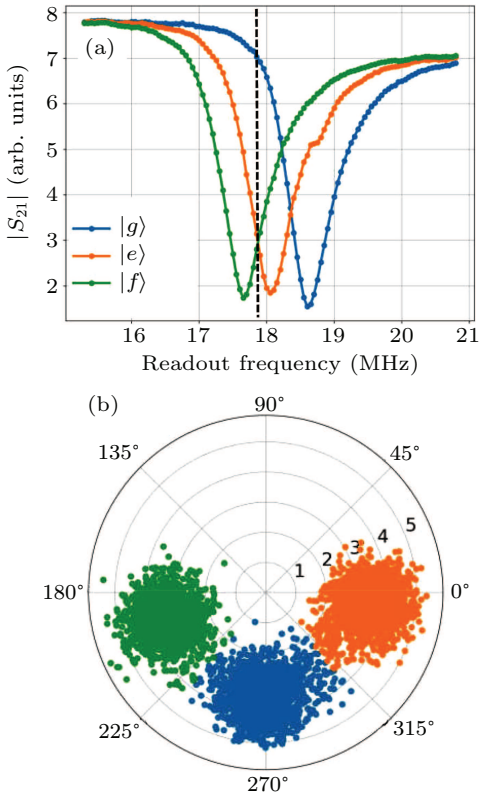


Fig. 3. (a) Transmission data measured when the qubit is in $|g\rangle$, $|e\rangle$ and $|f\rangle$ states, respectively. (b) Transmission data taken at a fixed frequency marked by the dashed line in (a).

In addition to the above parameters, the decay rates of the excited states γ_e and γ_f (representing decaying from the $|e\rangle$ and $|f\rangle$ states to environment) are of significance in the study of the non-Hermitian system. To characterize γ_e and γ_f, we need to firstly readout and distinguish the different states. According to the dispersive readout theory, we know that different qubit states correspond to different frequency shifts of the readout resonator frequency. In this way, we can distinguish the three states of interest $|g\rangle$, $|e\rangle$ and $|f\rangle$. The data are shown in Fig. 3. We use one π pulse or two sequential π pulses to prepare the qubit into $|e\rangle$ and $|f\rangle$ states, respectively. The transmission data measured on the readout transmission line are shown in Fig. 3(a). Clearly, the resonant frequency shows a state-dependent shift (Note, the frequencies displayed on the horizontal axis are the values after down conversation. The actual value should be added 6.61 GHz, the local oscillation frequency). In Fig. 3(b), we show the transmission data measured at a fixed frequency (as marked by the black dashed line) in the I–Q polar plane. The frequency is chosen so that the distinction of the three states is clear.

In practical measurements, the readout fidelity of a qubit state may be compromised by a number of factors such as decoherence, external interference, and is usually smaller than one hundred percent. We may use an operator matrix $\boldsymbol{M}_{\rm op}$ to account for the errors and the ideal probability may be obtained with $P_{\rm ideal} = \boldsymbol{M}_{\rm op}^{-1} \cdot P_{\rm actual}$. We prepare the qubit into $|g\rangle$, $|e\rangle$ and $|f\rangle$ states, respectively and compare the measured probabilities to those of the ideal cases. The $\boldsymbol{M}_{\rm op}$ is obtained as

$$M_{\rm op} = \begin{bmatrix} 0.988 & 0.098 & 0.026 \\ 0.012 & 0.891 & 0.105 \\ 0.00 & 0.011 & 0.869 \end{bmatrix}.$$

The relaxation of a multiple level system has been discussed in Ref. [31]. When the initial state is in the $|f\rangle$ state, the time evolution of occupation probability for $|g\rangle$, $|e\rangle$ and $|f\rangle$ states is

$$\begin{aligned} P_g(t) &= c_1 - c_2\,\mathrm{e}^{-\Gamma_{eg}t} + c_3 c_1\,\mathrm{e}^{-(\Gamma_{fg}+\Gamma_{fe})t}, \\ P_e(t) &= c_2\,\mathrm{e}^{-\Gamma_{eg}t} - c_2\,\mathrm{e}^{-(\Gamma_{fg}+\Gamma_{fe})t}, \\ P_f(t) &= c_3\,\mathrm{e}^{-(\Gamma_{fg}+\Gamma_{fe})t}. \end{aligned} \tag{9}$$

Among them, $c_3 = 1$, $c_2 = -c_3\Gamma_{fe}/(\Gamma_{eg} - \Gamma_{fg} - \Gamma_{fe})$, $c_1 = c_2 - c_3(-\Gamma_{eg} + \Gamma_{fg})/(\Gamma_{eg} - \Gamma_{fg} - \Gamma_{fe})$. Γ_{eg}, Γ_{fe}, Γ_{fg} are decay rates from $|e\rangle$ to $|g\rangle$, from $|f\rangle$ to $|e\rangle$, and from $|f\rangle$ to $|g\rangle$, respectively. By fitting the experimental data, shown in Fig. 4, to these relations, we obtain the decay rates, $\Gamma_{eg} = 0.18$ MHz, $\Gamma_{fg} = 0.006$ MHz, $\Gamma_{fe} = 0.0628$ MHz. According to Section 2, we know $\gamma_{e=}\Gamma_{eg}$ and $\gamma_f = \Gamma_{fg} + \Gamma_{fe}$.

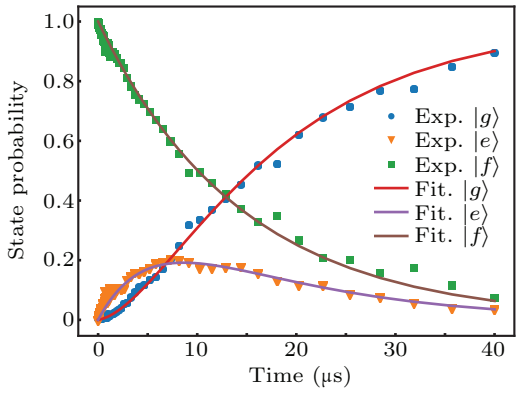


Fig. 4. Relaxation data measured for the three states $|e\rangle$, $|g\rangle$ and $|f\rangle$. The solid curves are fitting to Eq. (9).

4. Experimental control of qubit decay rate

According to Section 2, changing the coupling strength and detuning frequency between the qubit and resonator by

LFM leads to the changing of the qubit decay rate. This means that we can control the qubit decay rate by changing the amplitude and frequency of LFM. In our experiments, the bandwidth of the Z control line is limited to 0–500 MHz while the readout resonator frequency is 924 MHz greater than the quibt transition frequency when biased at the idle point. Thus, we may apply a LFM with modulation frequency around 462 MHz to achieve a large γ_e. This corresponds to $n = 2$ in Eq. (8). We prepare the qubit to the $|e\rangle$ state before applying LFM for 1 μs and finally measure the probability of state $|e\rangle$, P_e. We vary the LFM amplitude and frequency progressively to find the dependence of the decay rate on the LFM frequency and amplitude. The data are shown in Fig. 5 and the strip-like region with very low P_e, and hence large γ_e, is clearly identified.

When LFM is applied at the sweet point of the qubit, there is a DC bias component acting on the qubit, resulting in the amplitude and frequency dependence of the low P_e region shown in Fig. 5. If LFM is applied away from the sweet point, the low P_e region should be less frequency dependent.

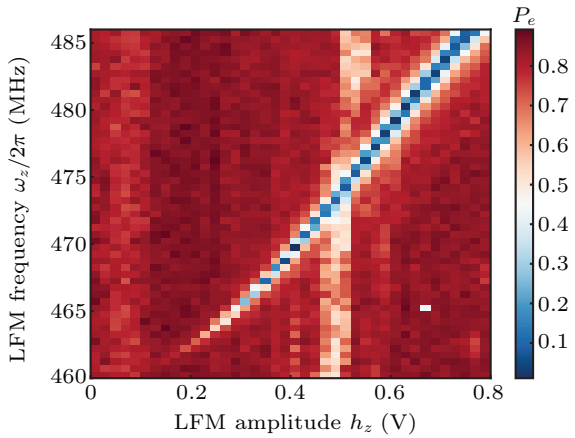


Fig. 5. The P_e data corresponding to different LFM h_z and ω_z.

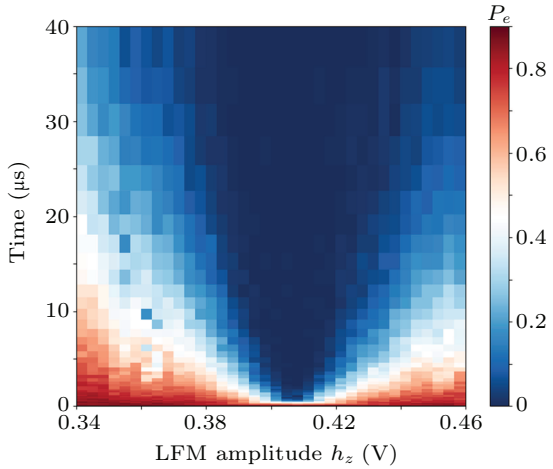


Fig. 6. Color map of P_e versus t for various values of h_z.

To show more clearly that γ_e changes with LFM, we fix a modulation frequency $\omega_z = 470$ MHz/2π and measure the γ_e for each modulation amplitude h_z. The result is shown in Fig. 6, and it is clear to see that γ_e changes with h_z.

After showing that the γ_e changes with h_z, we should also verify that γ_f does not change with h_z. As discussed in Section 3, we prepare the qubit to the state $|f\rangle$, and wait for some time, finally measure the probability of $|g\rangle$, $|e\rangle$, $|f\rangle$ states, respectively. During the waiting time, the longitudinal field is applied through the Z control line. According to Eq. (9), we can get γ_e and γ_f by fitting the probability data of $|g\rangle$, $|e\rangle$, and $|f\rangle$ states. Data shown in Fig. 7 confirm that the change of γ_f is small when LFM is applied. The red solid line is the fitting curve using Eq. (5). Note that the x-axis variable in Fig. 7 is $\Delta\omega$, the detuning of the qubit $n = 2$ sideband frequency to the readout resonator. In our experiments, the qubit is biased at the sweet point, thus the change of LFM amplitude h_z would also result in a change in $\Delta\omega$. However, if the change of h_z is small, the relation between the two is approximately linear.

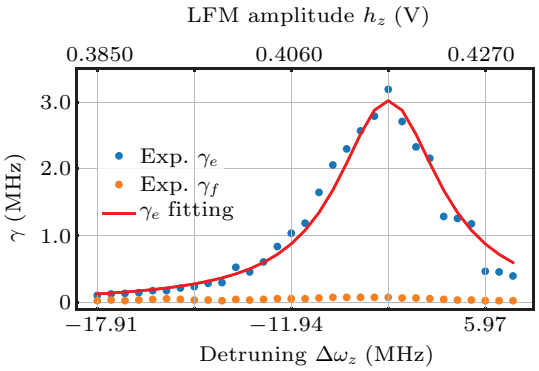


Fig. 7. The experiment results of γ_e and γ_f obtained by fitting the original relaxation data, similar to those shown in Fig. 4.

5. Quantified EP by oscillation frequency

To observe PT symmetry broken transition, we choose a working point at which γ_e is much larger than γ_f. Similar to the procedure described in Ref. [26], we apply π_{ge} and π_{ef} pulses to prepare the qubit to state $|f\rangle$ and then apply a coherent microwave driving in resonance with the $|e\rangle$ and $|f\rangle$ transition frequency and with amplitude J through the XY control line. In the same time, a LFM is also applied to the qubit via the Z control line so that γ_e is about 2.06 MHz and γ_f is about 0.08 MHz. Finally, after a period of time t, we switch off the driving field and LFM, and measure the occupation probability of state $|f\rangle$ P_f together with the probability of the state $|g\rangle$ and $|e\rangle$. The schematic diagram of the whole process is shown in Fig. 2(c). As discussed in Subsection 2.1, when $J > \gamma_e/4$, the system is in the PT symmetric phase and P_f would oscillate at a frequency

$$\Omega_0 = 2\,\mathrm{Re}(\sqrt{J^2 - J_0^2}). \tag{10}$$

At the EP, $J = \gamma_e/4$, the oscillation disappears.

Because we consider only the system formed with $|e\rangle$ and $|f\rangle$, we use the normalized probability $P_f^{\rm n} = P_f/(P_f + P_e)$ dynamics of the system. The results are displayed in Fig. 8. In Fig. 9(a), more detailed data are shown and the time dependence of $P_f^{\rm n}$ for two different J values (as marked by dashed lines in Fig. 9(a)) is given in Fig. 9(b). The solid lines are the fitting curves using a cosine function with exponentially decayed amplitude. Clearly, when J is large, we observe the oscillatory behavior of $P_f^{\rm n}$ and the oscillation disappears when J is reduced below a certain value.

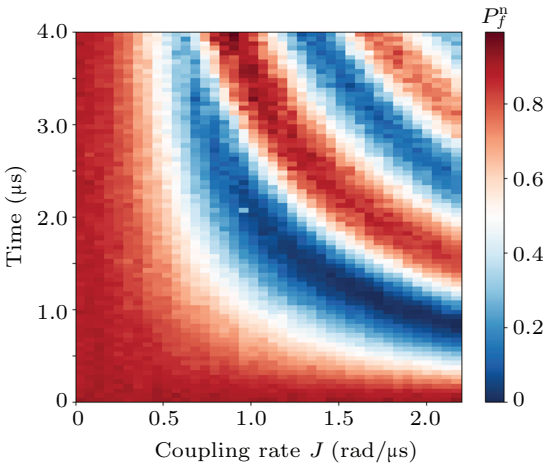


Fig. 8. Color map of $P_f^{\rm n}$ versus t for various values of J.

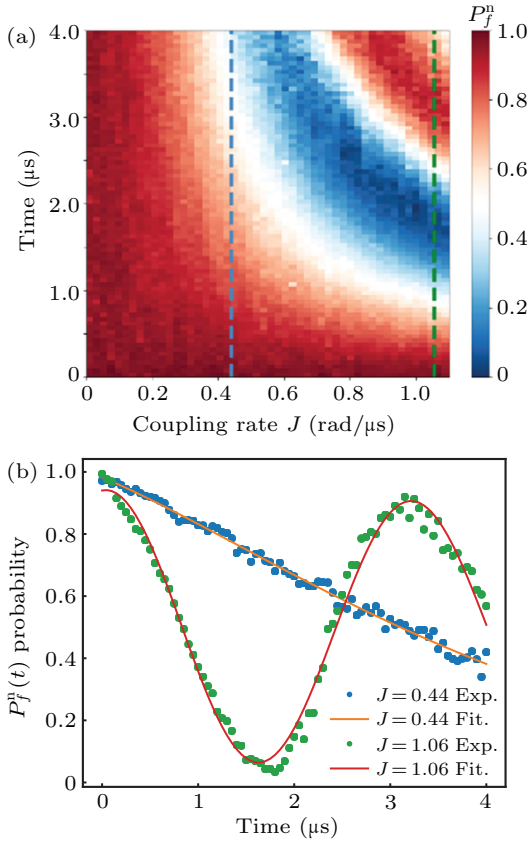


Fig. 9. (a) More detailed of $P_f^{\rm n}$ evolution data measured under the same condition as in Fig. 8. (b) The $P_f^{\rm n}$ versus time and the fitting plot for two values of J ($J = 106$, green dot; $J = 0.44$, blue dot).

In Fig. 10, the oscillation frequency Ω_0 obtained by fitting is exhibited as a function of coupling strength J. The point at which Ω_0 becomes zero is the EP. Further reducing J, the system is in the PT broken phase. The solid red line is the fit to Eq. (10). The data show that, at the EP, J_0 is about 0.46 rad/μs, being consistent with the value 0.51 rad/μs obtained from $\gamma_e/4$.

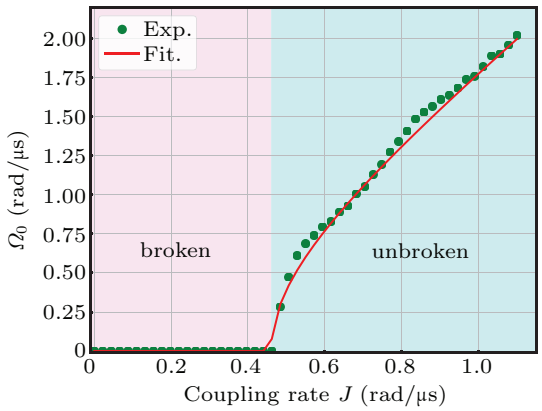


Fig. 10. Variation of oscillation frequency Ω_0 with coupling strength J.

6. Quantified EP through all parameter regions

It has been pointed out that to accurately determine the location of EPs in experiments by measuring the asymptotic behavior of the energy around the EP without special prior knowledge is difficult.[29] Indeed, the evolution of P_f under $H_{\rm eff}$ gives an exponential decay that makes the determination of Ω_0 become increasingly difficult when approaching the EP. To solve this problem, an alternative scheme of determining EP using all parameter regions has been proposed.[29] Here we also use this scheme in our experiments of superconducting qubits.

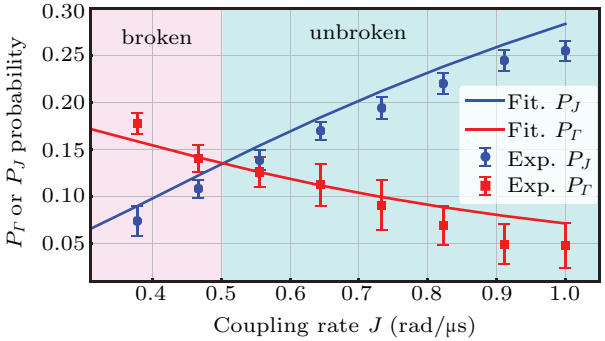


Fig. 11. Determination of EP from the measurement of P_J (blue) and P_Γ (red).

The specific operation and measurement procedures are as follows. (i) Prepare the initial state to $|f\rangle$ and let the system evolve for a period of time t. Then we measure the probability of state $|e,\rangle P_J(t)$. (ii) Repeat the procedure for the initial state $(|f\rangle + |e\rangle)/2$ and measure the probability of state $(|f\rangle - |e\rangle)/2$, $P_\Gamma(t)$. (iii) We repeat (i) and (ii) for different values of the coupling strength J and let $t = 1/J$. The data are

displayed in Fig. 11. The solid curves are fitting to the theoretical expression given in Ref. [29] which suggests that the cross point of P_J and P_Γ is the EP. At this point, we have $J_0 \sim 0.5$, being also consistent with the value obtained in Fig. 10.

This method does not need to fit the oscillation frequency to determine the EP. However, it utilizes information of all three states and hence requires better readout calibration of the three states and the fidelity of the operation.

7. Dependence of EP position on the decay rate

According to Subsection 2.1, the position of the EP should vary with the decay rate γ_e. We make measurements for four different values of γ_e and determine the corresponding EPs. The position of EP J_0 is shown in Fig. 12. The agreement between experiment points and $\gamma_e/4$ is reasonable.

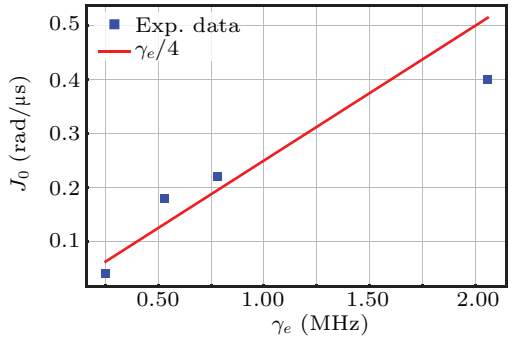


Fig. 12. Dependence of EP position J_0 on the decay rate γ_e.

8. Conclusion

We utilize a previously reported dissipation control technique for frequency tunable superconducting transmon qubits[30] to investigate the PT symmetric phase transition of non-Hermitian quantum system and determine the corresponding EP. The non-Hermitian quantum system is formed with the first and the second excited states of the qubit. We show that the dissipation rate of the first excited state of the transmon qubit could be tuned by parametric modulation of the qubit frequency. The parametric modulation effectively changes the coupling strength between the qubit and its lossy readout resonator. By varying the coupling between the two excited states of the qubit, the PT phase transition is observed. Two methods are used to determine the EP and the results are in agreement with that calculated by the theory.

Our study demonstrates a possible new approach for further investigation of the remarkable phenomena of non-Hermitian systems in the vicinity of the EP. Furthermore, the approach can be implemented on multi-qubit devices to investigate the properties of many-body non-Hermitian systems and to explore the high-order EPs.

References

[1] El-Ganainy R, Makris K G, Khajavikhan M, Musslimani Z H, Rotter S and Christodoulides D N 2018 *Nat. Phys.* **14** 11
[2] Özdemir S K, Rotter S, Nori F and Yang L 2019 *Nat. Material* **18** 783
[3] Lin Z, Ramezani H, Eichelkraut T, Kottos T, Cao H and Christodoulides D N 2011 *Phys. Rev. Lett.* **106** 213901
[4] Zheng A, Zhang G Y, Chen H Y, Mei T T and Liu J B 2017 *Scientific Reports* **7** 14001
[5] Ramezani, H, Kottos T, El-Ganainy R and Christodoulides D N 2010 *Phys. Rev. A* **82** 43803
[6] Peng B, Özdemir S K, Lei F, Monifi F, Gianfreda M, Long G L, Fan S H, Nori F, Bender C M and Yang L 2014 *Nat. Phys.* **10** 394
[7] Chang, L, Jiang X S, Hua S Y, Yang C, Wen J M, Jiang L, Li G Y, Wang G Z and Xiao M 2014 *Nat. Photo.* **8** 524
[8] Guo, A, Salamo G L, Duchesne D, Morandotti R, Volatier-Ravat M, Aimez V, Siviloglou G A and Christodoulides D N 2009 *Phys. Rev. Lett.* **103** 093902
[9] Brandstetter M, Liertzer M, Deutsch C, Klang P, Schöberl J, Türeci H E, Strasser G, Unterrainer K and Rotter S 2014 *Nat. Commun.* **5** 4034
[10] Peng B, Özdemir S K, Rotter S, Yilmaz H, Liertzer M, Monifi F, Bender C M, Nori F and Yang L. 2014 *Science* **346** 328
[11] Hodaei H, Hassan A, Wittek S, Garcia-Gracia H, El-Ganainy R, Christodoulides D N and Khajavikhan M 2017 *Nature* **548** 187
[12] Chen W, Özdemir S K, Zhao G M, Wiersig J and Yang L 2017 *Nature* **548** 192
[13] Regensburger A, Bersch C, Miri M A, Onishchukov G, Christodoulides D N and Peschel U 2012 *Nature* **488** 167
[14] Li L Z, Cao Y, Zhi, Y Y, Zhang J J, Zhou Y T, Feng X H, Guan B O and Yao J P 2020 *Sci. Appl.* **9** 169
[15] Lee S B, Yang J, Moon S, Lee S Y, Shim J B, Kim S W, Lee J H and An K 2009 *Phys. Rev. Lett.* **103** 134101
[16] Zhu J G, Özdemir Ş K, He L and Yang L 2010 *Opt. Express* **18** 23535
[17] Peng B, Özdemir Ş K, Liertzer M, Chen W J, Kramer J H, Yılmaz H, Wiersig J, Rotter S and Yang L 2016 *Proc. Natl. Acad. Sci. USA* **113** 6845
[18] Xu H, Mason D, Jiang L Y and Harris J G E 2016 *Nature* **537** 80
[19] Djorwe P, Pennec Y and Djafari-Rouhani B 2019 *Phys. Rev. Appl.* **12** 024002
[20] Wang B, Liu Z X, Kong C, Xiong H and Wu Y 2019 *Optics Express* **27** 8069
[21] Li J M, Harter A K, Liu J, Melo L D, Joglekar Y N and Luo L 2019 *Nat. Commun.* **10** 855
[22] Jiang Y, Mei Y F, Zuo Y, Li J S, Wen J M and Du S W 2019 *Phys. Rev. Lett.* **123** 193604
[23] Xu J, Du Y X, Huang W and Zhang D W 2017 *Opt. Express* **25** 15768
[24] Liu W Q, Wu Y, Duan C K, Rong X and Du J F 2021 *Phys. Rev. Lett.* **126** 170506
[25] Wu Y, Liu W Q, Geng J P, Song X R, Ye X Y, Duan C K, Rong X and Du J F 2019 *Science* **364** 878
[26] Naghiloo M, Abbasi M, Joglekar Y N and Murch K W 2019 *Nat. Phys.* **15** 1232
[27] Partanen M, Goetz J, Tan K Y, *et al.* 2019 *Phys. Rev. B* **100** 134505
[28] Wang W C, Zhou Y L, Zhang H L, *et al.* 2021 *Phys. Rev. A* **103** L020201
[29] Ding L Y, Shi K Y, Zhang Q X, Shen D N, Zhang X and Zhang W 2021 *Phys. Rev. Lett.* **126** 083604
[30] Zhou Y, Zhang Z X, Yin Z L, *et al.* 2021 arXiv:2103.11315
[31] Peterer M J, Bader S J, Jin X, Yan F, Kamal A, Gudmundsen T J, Leek P J, Orlando T, Oliver W and Gustavsson S 2015 *Phys. Rev. Lett.* **114** 010501
[32] Mostafazadeh A 2002 *Math. Phys.* **43** 205